A modeling approach integrating microbial activity, mass transfer, and geochemical processes to interpret biological assays: An example for PCE degradation in a multi-phase batch setup

Murray, Alexandra Marie; Maillard, Julien; Jin, Biao; Broholm, Mette Martina; Holliger, Christof; Rolle, Massimo

Published in:
Water Research

Link to article, DOI:
10.1016/j.watres.2019.05.087

Publication date:
2019

Document Version
Peer reviewed version

This is a Post Print of the article published online 27th May 2019 in Water Research. The publishers' version is available at the permanent link:
https://doi.org/10.1016/j.watres.2019.05.087

A modeling approach integrating microbial activity, mass transfer, and geochemical processes to interpret biological assays: An example for PCE degradation in a multi-phase batch setup

Alexandra Marie Murray[a], Julien Maillard[b], Biao Jin[c], Mette M. Broholm[a], Christof Holliger[b], and Massimo Rolle[a*]

[a]Department of Environmental Engineering, Technical University of Denmark, Kgs. Lyngby, DK-2800, Denmark

[b]Laboratory for Environmental Biotechnology, ENAC-IIE, Ecole Polytechnique Fédérale de Lausanne, 1015 Lausanne, Switzerland

[c]State Key Laboratory of Organic Geochemistry, Guangzhou Institute of Geochemistry, Chinese Academy of Science, China

Highlights

- Modeling approach integrating mass transfer, geochemistry, and microbial activity
- Quantified PCE degradation in the presence of iron- and sulfate-reducers
- Model validated with hydro-chemical and T-RFLP data
- Flexible tool for experimental design and comprehensive interpretation

Abstract

The rate at which organic contaminants can be degraded in aquatic environments is not only dependent upon specific degrading bacteria, but also upon the composition of the microbial community, mass transfer of the contaminant, and abiotic processes that occur in the environment. In this study, we present three-phase batch experiments of tetrachloroethene (PCE) degradation by a consortium of organohalide-respiring bacteria, cultivated alone or in communities with iron- and/or sulfate-reducers. We developed a modeling approach to quantitatively evaluate the experimental results, comprised of chemical and biomolecular time series data. The model utilizes the IPhreeqc module to couple multi-phase mass transfer between gaseous, organic and aqueous phases with microbial and aquatic geochemical processes described using the geochemical code PHREEQC. The proposed approach is able to capture the contaminant degradation, the microbial population dynamics, the effects of multi-phase kinetic mass transfer and sample removal, and the geochemical reactions occurring in the aqueous phase. The model demonstrates the importance of aqueous speciation and abiotic reactions on the bioavailability of the substrates. The model-based interpretation allowed us to quantify the reaction kinetics of the different bacterial guilds. The model further revealed that the inclusion of sulfate-reducing bacteria lowers the rate of PCE degradation and that this effect is moderated in the presence of iron-reducing bacteria.

1. Introduction

Biodegradation of organic contaminants in aquatic systems depends not only on the activity and metabolic capabilities of specific degraders but also on microbial community interactions and on the coupling with mass transfer processes and aquatic chemistry. Microbial community function determines the fate of organic chemicals both in natural systems such as groundwater aquifers, riverbed sediments and hyporheic zones (Hamonts et al., 2012; Meckenstock et al., 2015; Weatherill et al., 2018), and in engineered applications, including *in-situ* bioremediation

interventions and wastewater treatment plants (e.g., Wells et al., 2011). Physical processes such as mass transfer between different phases, diffusion and hydrodynamic dispersion are also of key importance since they can be the rate-limiting step and thus the bottleneck for the degradation of organic compounds (e.g., Bauer et al., 2009a; Rolle et al., 2010; Rolle and Kitanidis, 2014; Thullner et al., 2012). Further control on contaminant biodegradation occurs through the feedback between microbial activity and abiotic reactions, including aqueous chemical speciation and precipitation/dissolution of reactive minerals (e.g., Appelo and Postma, 2005; Postma and Jakobsen, 1996; Prommer et al., 2009).

Chlorinated ethenes are organic contaminants of primary concern that are widespread in groundwater aquifers and threaten the health of riverbed sediments and surface water bodies (Imfeld et al., 2008; Schneidewind et al., 2014; Weatherill et al., 2018; Xu et al., 2019). The most important degradation pathway of chlorinated ethenes is reductive dehalogenation by organohalide-respiring bacteria (OHRB), which can sequentially degrade the mother compounds such as tetrachloroethene (PCE) and trichloroethene (TCE), to daughter products *cis*-dichloroethene, vinyl chloride, and ultimately to the non-toxic ethene. This respiration process has been studied for more than two decades (Holliger et al., 1993), yet furthering understanding of how the interaction between microbial guilds, physical transport processes, and chemical reactions influences degradation kinetics can elucidate the functioning of degrader communities and will be instrumental to optimize bioremediation efforts.

Studying these systems *in situ* is difficult because microbial communities with relatively low biodiversity, such as those in groundwater sediments, can contain multiple thousands of taxa (Kotik et al., 2013). Hence, experimental studies with controlled conditions can increase our understanding of the interactions between different bacterial guilds (Marcus et al., 2013; Yu and Semprini, 2002). Cultivation of anaerobic microorganisms, both as pure cultures and as communities, is commonly

done in small, septum-sealed, anoxic batches (Abe et al., 2009; Amos et al., 2007; Yu and Semprini, 2004). These systems allow for the bacterial community members to intermingle in the aqueous phase, which is key for microbial interactions, such as commensalistic OHRB-containing communities, in which the OHRB are dependent upon fermenting bacteria for production of electron donor. Another benefit of these systems is that a separate phase, such as a non-aqueous phase liquid or a gaseous atmosphere containing a toxic compound or a substrate, can be added to the setup. For organic contaminants such as chlorinated ethenes, an immiscible organic layer can be added to the system; the high partition coefficients for PCE and TCE means that these compounds preferentially remain in the organic phase, yet as organisms in the aqueous phase consume these chemicals, a chemical gradient is maintained and the organic layer acts as a source and slowly releases more substrate to the aqueous phase (Buttet et al., 2018; Holliger et al., 1993). Such slow, mass transfer limited release allows addressing the issue of bacterial inhibition by the toxicity of high substrate concentrations and increasing the experimental duration (Daugulis, 2001; Déziel et al., 1999).

These experimental systems are useful, but determining microbial kinetic parameters, such as affinity constants and maximum substrate utilization rates without accounting for the physical characteristics of the experimental system would lead to erroneous interpretation (Buttet et al., 2018). When substrate is meted out to the bacteria slowly and continuously, mass transfer across the phase boundaries (e.g., aqueous-organic and organic-gaseous) impacts the apparent substrate utilization rate, just as mass transfer limits bioavailability in natural systems (Aeppli et al., 2009; Bauer et al., 2009a; Kampara et al., 2008; Thullner et al., 2008). Sequential sampling also impacts the mass balance in the system. If an experimental system is small or if the amount of sample removed is relatively large, the removal of mass by this mechanism must also be considered since it

affects the distribution of the different fluid phases in the setup (Buchner et al., 2016; Buttet et al., 2018).

Increasing the complexity of the bacterial community can also increase the complexity of the chemical reactions that occur in the aqueous phase (Gadd, 2010). To understand biodegradation kinetics one must determine the true concentration of the available substrate, thus the aqueous speciation of the substrates in the media needs to be accounted for. Furthermore, abiotic reactions between dissolved species and mineral precipitation/dissolution can impact microbial degradation processes. This is particularly important for microbial communities containing iron-reducing bacteria (FeRB) and sulfate-reducing bacteria (SRB), which entails that iron-sulfur geochemical reactions occur. Although the focus is often the microbial degradation of the organic contaminants, there is continuous feedback between the aquatic geochemistry and microbial community that is essential to understanding community dynamics and, ultimately, the degradation process.

Although the experimental techniques described above are well-represented in the literature, the current state of numerical modeling for such systems does not cohesively incorporate these currently disparate elements. Modeling of multi-phase batch systems has previously been used to describe chlorinated ethene degradation and isotope fractionation, but these models do not include complex aquatic geochemistry (Aeppli et al., 2009; Buttet et al., 2018; Jin et al., 2013). Likewise, kinetic models to investigate batch or microcosm experiments of contaminant degradation and microbial communities account for neither mass transfer limitations nor the influence of sample removal on the determination of microbial kinetic parameters (Chambon et al., 2013; Jin and Rolle, 2016; Kouznetsova et al., 2010; Malaguerra et al., 2011; Wade et al., 2016).

In this study we present multi-phase microbial ecology experiments and a novel modeling tool used to interpret them that includes the description of mass transfer and geochemical processes. We

95 performed laboratory batch experiments to investigate the impact of iron (Fe(III)) and sulfate
96 reduction by FeRB and SRB on PCE reduction by an OHRB consortium containing *Candidatus*
97 Sulfurospirillum diekerktiae strain SL2-1. The experiments consisted of four batches of increasing
98 ecological complexity: the first batch consisted of the OHRB consortium cultivated alone, the
99 second and third batches consisted of the OHRB consortium cultivated with either the FeRB or
100 SRB, and the fourth batch consisted of all three guilds together. The proposed modeling approach is
101 a coupling between a MATLAB®-based mass transfer code (Buttet et al., 2018) and the widely used
102 geochemical code PHREEQC (Parkhurst and Appelo, 2013). We demonstrate the utility of this
103 modeling tool to quantitatively interpret the experimental observations yielded by each batch,
104 including both chemical and molecular data. The model allowed us to: (i) elucidate the impact of
105 SRB and FeRB on PCE degradation, (ii) quantify the respiration kinetics of the different bacterial
106 guilds, and (iii) disentangle the contribution of the different physical, biological, and chemical
107 processes that occur in the multi-phase batch systems to the experimental observations, which
108 consisted of measured time series of chemical and biomolecular data.

109 ## 2. Materials and methods

110 ### 2.1 Experiment

111 #### 2.1.1 Cultures

112 The OHRB consortium, SL2-PCEc, that was used in this study originated from a chlorinated
113 ethene-contaminated aquifer and was enriched and maintained over several years (Buttet et al.,
114 2013). The consortium contains *Candidatus* Sulfurospirillum diekertiae, which is capable of
115 respiring PCE to TCE. The FeRB used in the experiments was *Shewanella oneidensis* strain MR-1
116 (Heidelberg et al., 2002); the SRB used was *Desulfovibrio vulgaris* Hildenburough (Heidelberg et
117 al., 2004). *S. oneidensis* and *D. vulgaris* were selected as model FeRB and SRB, respectively,

because both can use hydrogen and neither can use acetate as an electron donor (Fredrickson et al., 2008; Tang et al., 2007; Tao et al., 2014).

2.1.2 Experimental setup

The base medium used was phosphate-bicarbonate buffered with a low chloride concentration (Holliger et al., 1993), the composition is listed in detail in Table S1. Medium components (chemicals sourced from Sigma-Aldrich Chemie GmbH, Buchs, Switzerland) and concentrated stocks were prepared with milliQ water and either autoclaved for 20 min at 121 ºC or filtered through 0.22 µm sterile filters. All medium components were added to 125-mL autoclaved bottles sealed with butyl rubber stoppers using sterile syringes. Aliquots of 45 mL of base medium were prepared, and acetate, Fe(III)-citrate, and sulfate stock solutions were each added such that in the finished medium, 2 mM of carbon source, 5 mM of Fe(III) source, and 5 mM of sulfate source were present. The headspace was replaced with a 4:1 mixture of hydrogen to carbon dioxide through 0.22 µm sterile filters. The initial starting pressure of each bottle was approximately 1.5 atm; hydrogen was added to each batch in excess, and microbial activity is limited by the availability of the electron acceptor in this study.

After the replacement of the headspace and before inoculation, 5 mL of 100 mM PCE dissolved in hexadecane was added to the system. Because hexadecane has a lower density than and is immiscible with water, the hexadecane formed an organic layer between the aqueous and gaseous compartments in the bottle. PCE has a hexadecane-water partition coefficient of approximately 5000, thus the pre-inoculation aqueous concentration was 20 µM (Holliger et al., 1993). The bottles were allowed to sit for 24 hours before inoculation, such that there was ample time for equilibration of PCE between the phases before introduction of the bacteria.

SL2-PCEc, *S. oneidensis*, and *D. vulgaris* were cultivated statically as separate inocula in a dark 37 ºC room. The same cell count of the relevant guilds was added to each batch. Inoculation of the experimental batches was timed such that all inocula were in the exponential growth phase. All batch experiments were grown in the same conditions as the inocula. All combinations were conducted with biological duplicates. Samples of 1.5 mL were removed for analytical and molecular analyses. The samples were taken at regular intervals, with no more than 12 hours between sample points, until constant chloride concentration values were obtained in all bottles, which occurred after 3.5 days.

2.1.3 Molecular Methods

Cell counts of each guild inoculum, in order to match cell counts of inocula, were quantified by quantitative polymerase chain reaction (qPCR) using the universal primers detailed in the Supplementary Information. Analysis of qPCR data was performed on a MIC apparatus (Bio Molecular Systems). A standard curve was run in duplicate, and all samples were run in triplicate. PCR and terminal restriction length polymorphism (T-RFLP) sample analysis for each experimental batch were completed as described in the Supplementary Information. Although the T-RFLP analysis does not give absolute cell count values, it allows tracking of the temporal evolution of the entire community and verification that no unexpected population from the OHRB consortium appears during the experimental duration. Fragment counts were converted into cell counts by adjusting for the number of 16S rRNA gene copies per genome for each species (1 gene copy $cell^{-1}$ for *S. diekertiae*, 5 gene copies $cell^{-1}$ for *D. vulgaris*, and 9 gene copies $cell^{-1}$ for *S. oneidensis*) (Buttet et al., 2018; Heidelberg et al., 2004, 2002).

2.1.4 Analytical Methods

Fe(II) concentrations were measured using a colorimetric ferrozine assay (Viollier et al., 2000). Samples for ferrozine assay analysis were diluted ten times in 0.5 M HCl directly upon removal to

prevent oxidation of Fe(II) to Fe(III) and to dissolve any Fe(II) precipitates (Zhou et al., 2017). Samples were not filtered, and thus the total Fe(II) concentration was measured. Chloride concentrations were determined via silver ion titration with a Chlor-o-counter (Flohr Instument, Nieuwegein, Netherlands). Because SL2-PCEc is only capable of transforming PCE to TCE, produced chloride is attributable to this single dechlorination step and PCE degradation can be measured without chlorinated ethene quantification (Buttet et al., 2018). Sulfate was measured by ion chromatography – suppressed conductivity detection (ICS-5000, Thermo Fisher). Samples were pretreated by passing them through a cleanup-cartridge (1 cc, Dionex OnGurad II Na, ThermoScientific) to remove divalent metal ions and protect the column and suppressor. Samples for sulfate analysis were diluted five times in a 5% zinc acetate solution directly upon removal to trap sulfide as zinc sulfide. Samples for sulfate analysis were frozen at -20ºC until analysis.

2.2 Modeling Approach

The conceptual arrangement of the bacterial, multi-phase mass transfer, and aquatic geochemical processes that occur in the multi-phase experimental setup are schematically represented in Figure 1. Mass transfer in the model is driven by both bacterial respiration (bolded and colored arrows, Figure 1) and sample removal (block arrow, Figure 1). In this section, we first describe each process individually and then present their combination in a modeling framework.

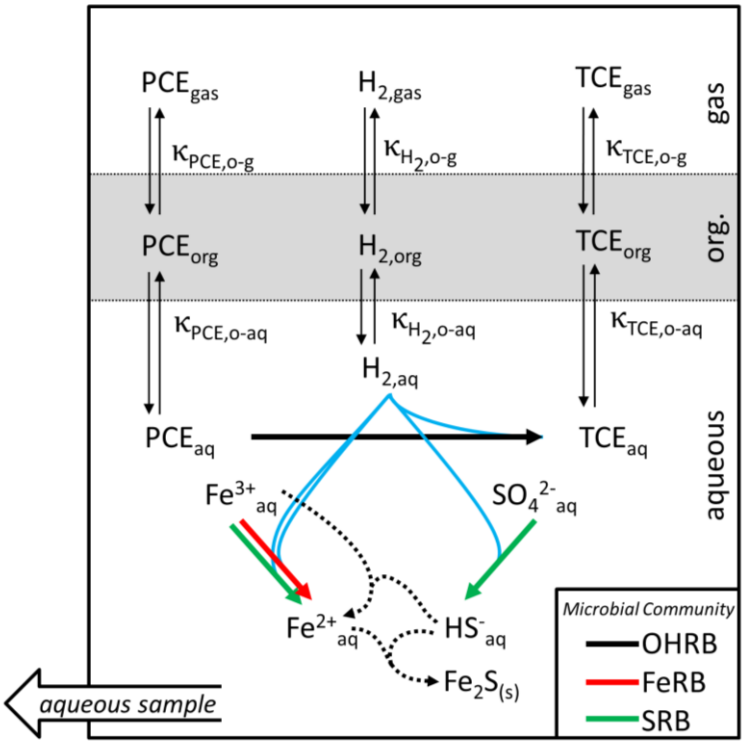

181

182 *Figure 1. Conceptual model of the physical, chemical, and bacterial processes that occur in the*
183 *experimental setup, where* $\kappa_{i,o\text{-}aq}$ *is the mass transfer coefficient between the organic and aqueous*
184 *phases, and* $\kappa_{i,o\text{-}g}$ *between the organic and gas phases, for compound i. The thick black arrow*
185 *represents respiration by the OHRB* Candidatus *Sulfurospirillum diekerktiae, the thick red arrow*
186 *respiration by the FeRB* Shewanella oneidensis*, and the thick green arrows respiration by the SRB*
187 Desulfovibrio vulgaris*. Blue arrows respresent pathways in which hydrogen is consumed. Slim*
188 *black arrows represent mass transfer across phase boundaries. Dotted black lines represent*
189 *aquatic geochemical reactions. The block arrow indicates that the aqueous phase is removed*
190 *during sampling.*

191

2.2.1 Bacterial Kinetics

The bacterial processes (bolded and colored arrows, Figure 1), are the primary driving force for mass transfer and transformations that occur during the experiment. Double Monod kinetics were used to simulate the consumption of both the electron donor and electron acceptors (Rittmann and McCarty, 2001):

$$\frac{dC_{aq,EA}}{dt} = -k_{max}X\left(\frac{C_{aq,ED}}{C_{aq,ED} + K_{S,ED}}\right)\left(\frac{C_{aq,EA}}{C_{aq,EA} + K_{S,EA}}\right) \quad (1)$$

where $dC_{aq,EA}/dt$ [mol L^{-1} h^{-1}] is the change in electron acceptor in the aqueous phase due to bacterial processes, $C_{aq,ED}$ and $C_{aq,EA}$ [µM] are the aqueous concentration of electron donor and acceptor, k_{max} [mol $cell^{-1}$ s^{-1}] is the maximum specific reduction rate, X [cells L^{-1}] is the biomass concentration, t [s] is time, and $K_{S,ED}$ and $K_{S,EA}$ [M] are the half-saturation constants for the electron donor and acceptor. The electron acceptors present in the media are PCE, Fe(III), and sulfate; hydrogen was the electron donor for all guilds. The change in substrate is related to biomass by:

$$\frac{dX}{dt} = Y_{EA}\frac{dC_{aq,EA}}{dt} - k_dX \quad (2)$$

where Y_{EA} [cells mol^{-1}] is the biomass yield on the electron acceptor and k_d [s^{-1}] is the linear decay coefficient. Equations 1 and 2 were applied for OHRB respiration of PCE to TCE, FeRB respiration of Fe(III) to Fe(II), and SRB respiration of sulfate to sulfide. *D. vulgaris*, the SRB used in the experiment, is also capable of respiring Fe(III). Elias et al. (2004) document this respiration to follow first-order kinetics, dependent only on the concentration of Fe(III), and both Elias et al. (2004) and Park et al. (2008) demonstrate that growth does not occur when reducing this metal ion. Fe(III) reduction by SRB was thus modeled by:

$$\frac{dC_{aq,Fe(III)}}{dt} = -k_{FeBio} C_{Fe(III),Bio} \quad (3)$$

where k_{FeBio} [s^{-1}] is the first-order rate constant. The SRB *D. vulgaris* is modeled as capable of respiring both aqueous Fe(III) and sulfate, depicted by the green arrows in Figure 1. The bioavailable Fe(III) is thus used as an electron acceptor by two guilds included in the experiments.

Table 1. Stoichiometry for respiration and cell synthesis half reactions

Reaction	**Stoichiometry**
R_{ED}	$\frac{1}{2}H_2 \rightarrow H^+ + e^-$
R_{Bio}	$\frac{1}{2}CH_3COO^- + \frac{1}{4}CO_2 + \frac{1}{4}NH_4^+ + \frac{5}{4}H^+ + e^- \rightarrow \frac{1}{4}C_5H_7O_2N + H_2O$
R_{EA}: PCE	$\frac{1}{2}C_2Cl_4 + H^+ + e^- \rightarrow \frac{1}{2}C_2HCl_3 + \frac{1}{2}H^+ + \frac{1}{2}Cl^-$
R_{EA}: Fe^{3+}	$Fe^{3+} + e^- \rightarrow Fe^{2+}$
R_{EA}: SO_4^{2-}	$\frac{1}{8}SO_4^{2-} + \frac{19}{16}H^+ + e^- \rightarrow \frac{1}{16}H_2S_{(g)} + \frac{1}{16}HS^- + \frac{1}{2}H_2O$

The hydrogen oxidation, cell synthesis, and PCE, Fe(III), and sulfate reduction half reactions (Table 1) were balanced using the method by Rittmann and McCarty (2001). The total stoichiometric reaction for each guild was obtained by a linear combination of the half reactions in Table 1:

$$R_{Total} = f_s(R_{Bio} + R_{ED}) + f_e(R_{EA} + R_{ED}) \quad (4)$$

where R_{Bio}, R_{ED}, and R_{EA} are the half reactions for biomass synthesis, the electron donor, and the electron acceptor, respectively, and R_{total} is the combined reaction. f_s and f_e are the fractions of electrons utilized for cell synthesis and energy production, respectively, which are calculated based on the yield factor, Y_{EA}, expressed as [$mol_{biomass}$ mol^{-1}]. Moles of biomass are assumed to be represented by the formula $C_5H_7O_2N$ (Holliger et al., 1993) and each cell to have a mass of 1.72×10^{-13} g $cell^{-1}$ (Balkwill et al., 1988). Growth does not occur during Fe(III) respiration by SRB, thus f_s for this process is zero and all electrons are used for energy (f_e = 1). For all other reactions,

225 cell synthesis was modeled to occur via the same stoichiometry for all bacterial guilds. It has been
226 found that approximately 70% of cell carbon for anaerobic bacteria is sourced from acetate and
227 approximately 30% from CO_2 (R_{Bio}, Table 1) (Badziong and Thauer, 1978; Holliger et al., 1993).
228 Fe(III) reduction by FeRB and SRB followed the same stoichiometry.

229 **2.2.2 Multi-phase Kinetic Mass Transfer**

230 The movement of the electron donor and acceptor between the phases are represented by the slim,
231 black arrows in the conceptual model (Figure 1). The differential equations 5, 6, and 7 describe the
232 change in concentration of each relevant compound in each compartment by kinetic mass transfer
233 (Aeppli et al., 2009; Jin et al., 2013):

$$\frac{dC_{aq,i}}{dt} = \frac{\left(\frac{dn_i}{dt}\right)_{gas-aq}}{V_{aq}} + \frac{\left(\frac{dn_i}{dt}\right)_{org-aq}}{V_{aq}} \quad (5)$$

$$\frac{dC_{org,i}}{dt} = \frac{-\left(\frac{dn_i}{dt}\right)_{org-aq}}{V_{org}} + \frac{-\left(\frac{dn_i}{dt}\right)_{org-gas}}{V_{org}} \quad (6)$$

$$\frac{dC_{gas,i}}{dt} = \frac{-\left(\frac{dn_i}{dt}\right)_{gas-aq}}{V_{gas}} + \frac{\left(\frac{dn_i}{dt}\right)_{org-aq}}{V_{gas}} \quad (7)$$

234 where $dC_{i,p}/dt$ [mol L^{-1} s^{-1}] is the change in concentration for the compound, i, in phase, p, V_p [L] is
235 the volume of phase p, and dn_i/dt [mol s^{-1}] is the total change in moles between phases for the
236 compound. PCE, TCE, and hydrogen were modeled to move between the phases, and movement
237 from the organic phase is defined as positive. Hydrogen concentrations were calculated based on the
238 known initial pressure in and fractional composition of the headspace and the ideal gas law. The
239 movement of mass across the two relevant phase interfaces, $(dn_i/dt)_{org\text{-}aq}$ and $(dn_i/dt)_{org\text{-}gas}$, is
240 described by Equations 8 and 9 (Aeppli et al., 2009):

$$\left(\frac{dn_i}{dt}\right)_{org-aq} = V_{aq}(C^{eq}_{aq,i} - C_{aq,i})\left(\frac{\kappa_{org-aq,i} \cdot A}{V_{org}}\right) \quad (8)$$

$$\left(\frac{dn_i}{dt}\right)_{org-gas} = V_{gas}(C^{eq}_{gas,i} - C_{gas,i})\left(\frac{\kappa_{org-gas,i} \cdot A}{V_{org}}\right) \quad (9)$$

where $C_{p,i}$ [M] and $C^{eq}_{p,i}$ [M] are the concentration and equilibrium concentration of compound *i* in phase *p*, $\kappa_{org\text{-}aq,i}$ [dm s^{-1}] and $\kappa_{org\text{-}gas,i}$ [dm s^{-1}] are the mass transfer coefficients for compound *i*, and *A* [dm^2] is the cross-sectional area of the phase interface. Mass transfer coefficients can be found in Table S2.

2.2.3 Sample Removal

Sample removal and re-equilibration of PCE, TCE, and hydrogen was also included in the model. Sampling removes substrate from the system, and it has previously been found to increase the chloride concentration in the aqueous phase above what would have been possible without removal of the aqueous phase (Buttet et al., 2018). Additionally, removal of phase volume from the system affects the pressure in the batch bottle. Equilibration of the volatile compounds was modeled as occurring instantaneously after sample removal. The total moles of the compound remaining in the system at time *t*, after sample removal, was calculated by subtracting the moles in the aqueous sample removed at time *t* from the moles present before removal at time *t-1*:

$$n_{i,t} = (C_{gas,i}V_{gas} + C_{org,i}V_{org} + C_{aq,i}V_{aq})_{t-1} - (C_{aq,i}V_{S,aq})_t \quad (10)$$

where $n_{i,t}$ [mol] is the remaining mass of compound *i* and $V_{S,aq}$ [L] is the volume of the removed sample. The concentrations of the compound in each phase after sample removal was then calculated (Buchner et al., 2016) using the partition coefficients $K_{gas\text{-}org}$ and $K_{org\text{-}aq}$ [-] (Table S2).

2.2.4 Geochemistry

The iron and sulfide chemistry in the aqueous phase both affects and is affected by the microbial reduction processes. The aqueous chemistry directly affects these bacterial processes via the speciation, and consequently the bioavailability, of the Fe(III) electron acceptor (Haas and Dichristina, 2002; Liu et al., 2001). Both the SRB and FeRB were modeled as only able to respire aqueous Fe(III) ions and the Fe(III) hydroxyl complexes $Fe(OH)_3$, $Fe(OH)_2^+$, and $Fe(OH)_4^-$. Fe(III) was added to the media as Fe(III)-citrate, which was modeled in PHREEQC to speciate according to the reactions included in Table 2.

Table 2. Fe(III)-citrate speciation reactions included in the PHREEQC database

Reaction	Log(k)
$Fe^{3+} + Citrate^{3-} + H_2O \rightarrow FeCitrateOH^- + H^+$	9.98[a]
$Fe^{3+} + Citrate^{3-} \rightarrow FeCitrate$	12.55[b]
$Fe^{3+} + 2Citrate^{3-} + H_2O \rightarrow FeCitrate_2OH^{4-} + H^+$	13.42[a]
$Fe^{3+} + Citrate^{3-} + H^+ \rightarrow FeCitrateH^+$	19.8[b]
$Fe^{3+} + 2Citrate^{3-} + 2H^+ \rightarrow FeCitrate_2H_2^-$	26.46[a]

[a]Reaction and log(k) as described in Liu et al. (2001)
[b]Reaction and log(k) from the PHREEQC minteq.dat database

Geochemical reactions in the system, depicted in Figure 1 as dotted lines, are also driven by the bacterial processes. Fe(III) reacts abiotically with sulfide, a product of sulfate reduction, by the stoichiometric reaction and rate kinetics described in Equations 11 and 12, respectively:

$$2Fe^{3+} + HS^- \rightarrow 2Fe^{2+} + S^0 + H^+ \quad (11)$$

$$\frac{dC_{Fe(II)}}{dt} = k_{FeAbio} C_{Fe(III)} C_{S(-II)}{}^{0.5} \quad (12)$$

where k_{FeAbio} [$L^{0.5}$ $mol^{-0.5}$ s^{-1}] is the kinetic rate constant for Fe(II) production as a result of abiotic Fe(III) reduction (Poulton et al., 2004; Rickard and Luther, 2007). The rate of abiotic Fe(III) reduction has been determined to be first order with respect to Fe(III) and 0.5 order with respect to

sulfide (Poulton et al., 2004). The produced Fe(II) then also reacts with sulfide to form amorphous $FeS_{(s)}$ that later crystalizes to mackinawite (Remoundaki et al., 2008; Zhou et al., 2017, 2014). When sulfide concentrations are high (10^{-5} M or greater) and the pH is neutral, Rickard (1995) found that this precipitation reaction proceeds by a reaction between Fe(II) and sulfide, where $FeS_{(s)}$ is formed via the intermediate $Fe(HS)_{2(s)}$ mineral with an empirically determined pseudo first-order sulfide disappearance rate of 15 s^{-1} (Rickard, 1995). Because the formation of the FeS precipitate is quick and the duration of the experiment was not long enough for crystalized mackinawite to form, amorphous $FeS_{(s)}$ was allowed to precipitate in the model at equilibrium via the reaction (Jakobsen, 2007):

$$Fe^{2+} + HS^- \rightarrow FeS_{(s)} + H^+ \quad (13)$$

where the log of the equilibrium constant, log(k), for $FeS_{(s)}$ was used from the PHREEQC geochemical database.

2.2.5 Coupling Strategy

The bacterial, mass transfer, consecutive sample removal, and aqueous chemistry modeling components are linked together via the scheme presented in Figure 2. Two software platforms are used, MATLAB® (R2017b) and PHREEQC-3 (Parkhurst and Appelo, 2013). The IPhreeqc module (Charlton and Parkhurst, 2011), allowing the use of PHREEQC with other codes and scripting languages (Muniruzzaman and Rolle, 2016; Van Breukelen et al., 2017; Wissmeier and Barry, 2011), was employed to interface the two software platforms. The mass transfer processes and re-equilibration after sample removal were performed in MATLAB®, analogous to the transport steps in reactive transport models using an operator splitting approach (e.g., Muniruzzaman and Rolle, 2016; Rolle et al., 2018). The state of the aqueous phase after these processes was then communicated to the PHREEQC geochemical code using the IPhreeqc module. All biogeochemical

processes including aqueous speciation, homogeneous and heterogeneous reactions, contaminant degradation and bacterial population dynamics were performed by PHREEQC. The flexible coupling strategy allowed us to perform simulations mimicking the steps taken in the laboratory experiments, as illustrated in Figure 2. First, the media was assembled and the volatile compounds equilibrated between all phases (Point A). The bacterial inocula were then added to each experimental batch (Point B), and an initial sample was removed and the volatile compounds re-equilibrated (Point C).

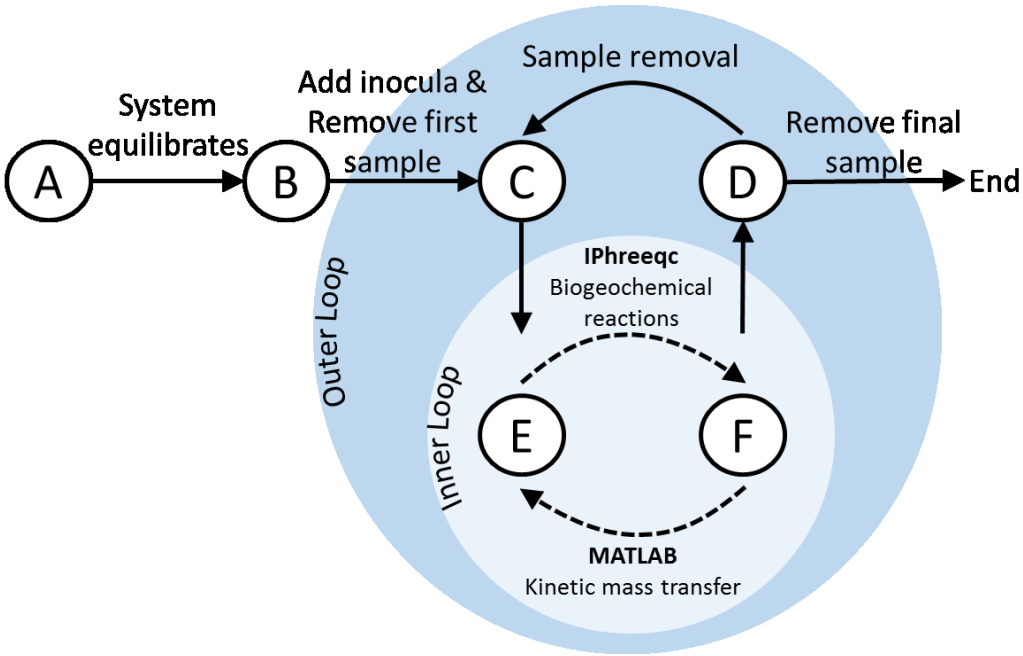

Figure 2. Coupling strategy for MATLAB® and PHREEQC software platforms; the bacterial and aqueous chemical procceses are computed using PHREEQC and the instantaneous and kinetic mass transfer processes are completed using MATLAB®. Solid black arrows denote steps that are modeled to occur instantaneously, and dashed arrows denote continuous processes that proceed for a defined time length.

Equilibration after the initial sample is removed begins the outer of two nested loops. The outer loop is organized in discrete segments, the length of which is defined by the time between the

312 experimental sampling events. Point D is prior to and Point C is directly after sample removal. To
313 move from Point C to D, the model enters the inner of the two nested loops. To return to Point C
314 from Point D, the volume of the aqueous phase is decreased by the size of the sample volume and
315 the volatile compounds are re-equilibrated between the phases.

316 After a sample is removed, the inner of the two nested loops begins. This inner loop is based on an
317 operator splitting scheme that alternates between the PHREEQC and MATLAB® platforms with a
318 small coupling time step (i.e., $\Delta t = 5s$). To move from Point E to F, the bacterial and geochemical
319 processes proceed in PHREEQC. After each time step, the model arrives to Point F, and the
320 concentrations of the volatile compounds in the aqueous phase are passed to MATLAB®, which
321 solves the set of differential equations to describe kinetic mass transfer between the phases with the
322 stiff solver *ode15s*. The concentrations of the volatile compounds are returned to PHREEQC at
323 Point E and the loop repeats. When the next sample is to be removed, the concentrations of the
324 volatile compounds at Point F are returned to MATLAB® at Point D, a sample is removed, and the
325 next iteration of the outer loop begins at Point C. Removal of the last sample signals the end of the
326 outer loop.

327 **2.2.6 Parameter Fitting**

328 The model was applied to the performed experiments to interpret the chemical and molecular data
329 in all the experimental batch setups that we have considered with the aim of quantifying the kinetics
330 of the different microbial guilds. As many parameters were chosen from the literature as possible to
331 limit the number of parameters to be fitted to the k_{max} for each guild's respiration process. Parameter
332 fitting was conducted within the MATLAB® environment using the function *lsqnonlin* (e.g.,
333 Haberer et al., 2015). The OHRB initial cell count was fitted for each experimental batch to account
334 for unknown activity of the inoculum, in which the upper bound was the measured initial count,
335 1.02×10^8 cells L^{-1}. k_{max} was fitted for all bacterial guilds in all experimental batches. In the batch

that included OHRB and FeRB, $K_{S,FeRB,Fe3}$ was also fitted, as values found in the literature were for the total dissolved Fe(III) concentration, not the easily bioavailable dissolved Fe(III) concentration (Liu et al., 2001). Parameters fit to describe 2-part community batch configurations, e.g., $K_{S,FeRB,Fe3}$ and k_{FeAbio}, were used as fixed inputs in subsequent, 3-part community batch simulations.

3. Results and Discussion

The four experimental configurations are detailed in Table 3. From left to right, each column gives the details of the batches as they increase in complexity. Batch 1, the single-community consisting of the OHRB consortium, is used to demonstrate the utility of the model as it relates to mass transfer across the phase boundaries and replicating sequential sample removal. Batch 2, the community consisting of OHRB and FeRB, shows how multiple guilds can be simulated. Aqueous speciation is modeled in all batches, and Batch 2 demonstrates that the Fe(III) bioavailability directly impacts iron respiration. Batch 3 is still comprised of two guilds, OHRB and SRB, and includes the complex aquatic geochemical processes that result from sulfate reduction products. Finally, Batch 4 is the most complex configuration, and consists of all three guilds and biogeochemical reactions considered. Data and simulations for each batch duplicate are included in the SI. In all simulations, the fitted initial cell count was found to vary in an interval spanning less than half an order of magnitude (i.e., with a minimum of 5.93×10^{7} cells L^{-1}), indicating the added cultures were proportionally and initially active.

Table 3. Overview of the experiments, including guilds added to the batch and the processes and data that are relevant to each batch

	Single Community	Two-part Community		Three-part Community
Batch	**1**	**2**	**3**	**4**
Guilds	OHRB	OHRB FeRB	OHRB SRB	OHRB FeRB SRB
Relevant Processes **Biotic**	PCE reduction	PCE reduction Fe(III) reduction (FeRB)	PCE reduction Sulfate reduction Fe(III) reduction (SRB)	PCE reduction Fe(III) reduction (FeRB) Sulfate reduction Fe(III) reduction (SRB)
Abiotic		Fe(III) speciation	Fe(III) speciation Fe(III) reduction $FeS_{(s)}$ precipitation	Fe(III) speciation Fe(III) reduction $FeS_{(s)}$ precipitation
Relevant Data	Chloride	Chloride Fe(II) T-RFLP	Chloride Fe(II) T-RFLP Sulfate	Chloride Fe(II) T-RFLP Sulfate

3.1 Single Community: Organohalide-Respiring Bacteria

In Batch 1, the OHRB consortium was cultivated without any other functional guild, and thus the chloride data is most relevant, as it is the product of PCE respiration. Repeated chloride concentration values from approximately 48 h indicate that all PCE consumption stopped at this time. The model was able to simulate the sigmoid curve of the measured chloride (Figure 3a) and thus capture PCE dechlorination to TCE and subsequent growth of OHRB. The $k_{max,PCE}$ for the OHRB in Batch 1 and its biological duplicate were 4.50×10^{-18} and 4.01×10^{-18} mol_{PCE} $cell^{-1}$ s^{-1} (Table 4), which is one order of magnitude greater than the average value found during previous experiments with the same consortium (Buttet et al., 2018) and also in other studies with members of the same organohalide-respiring genus (Aeppli et al., 2009; Scholz-Muramatsu et al., 1995). This can be attributed to the difference of electron donor, as formate was used as the electron donor in Buttet et al. (2018), and supply of hydrogen has been shown to best promote dechlorination (Aulenta et al., 2007).

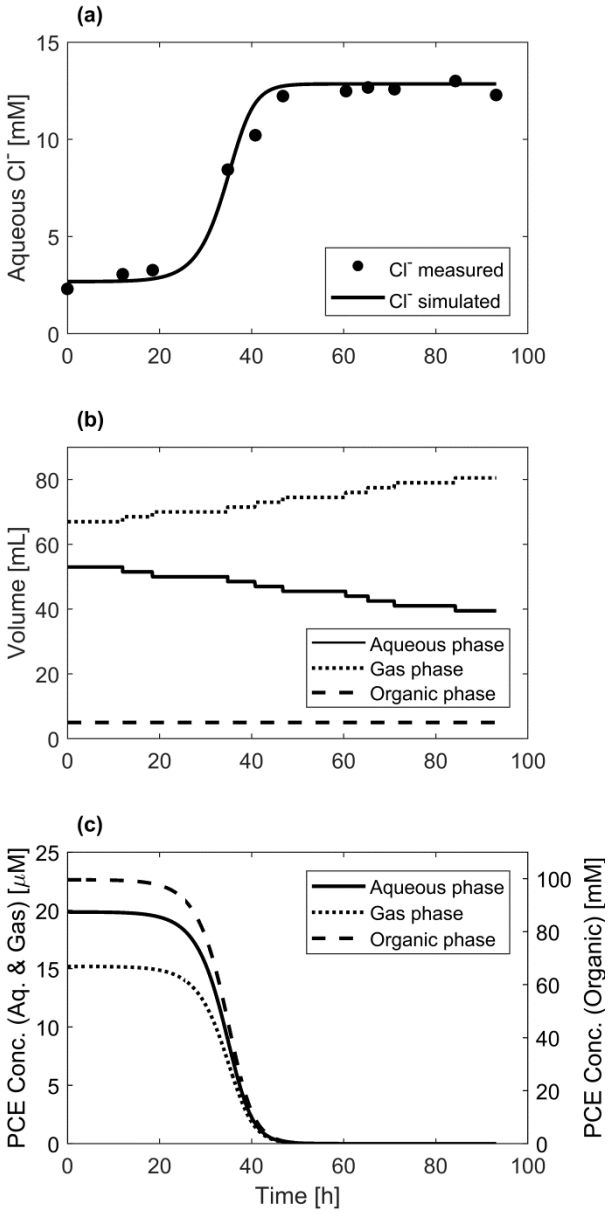

370

371 *Figure 3. OHRB only (Batch 1) experimental and simulated chloride aqueous concentration (a),*
372 *phase volume changes due to sampling (b), and simulated decrease of PCE in all phases (c). Data*
373 *and simulation results for the biological duplicate are included in the Supplementary Information*
374 *(Figure S1).*

375 Figure 3b depicts the calculated volume of each phase throughout the experiment. Even with a
376 minimal sampling volume of 1.5 mL, it is still evident that consecutive sampling has a considerable
377 impact on the phase volumes of the batch system. The initial volume of the aqueous phase

decreased by 18% (and the volume of the gas phase increased by the same volume) over the duration of the experiment. The initial pressure in the bottle was approximately 1.5 atm, determined when the headspace was exchanged prior to addition of the organic phase during preparation of the experiment. At the end of the experiment, because of sample removal and consumption of PCE and hydrogen, the calculated pressure in the batch was 1.0 atm. Additionally, the model allows us to track the evolution of the volatile species in all phases (Figure 3c, example for PCE). It was determined that the electron donor was present in excess in the aqueous phase; the lowest aqueous hydrogen concentration in the batch was 5.35×10^{-4} M. The model shows that the PCE concentration in all three phases is zero after approximately 48 h. This coincides with the repeated chloride concentration values and simulation (Figure 3a) that indicate PCE respiration has stopped, with complete PCE consumption in the system after 48 h.

3.2 Two-Part Community: Organohalide- and Fe(III)-Respiring Bacteria

In Batch 2, the two-part community composed of the OHRB consortium and FeRB (Table 3 Column 2), chloride and Fe(II) are respiration products that can be used as evidence of the functional guilds' metabolic activity. The chloride sigmoid data and simulation for Batch 2 is similar to Batch 1, with the OHRB alone, and repeated chloride concentration values were also observed after approximately 48 h. (Figure 4a).

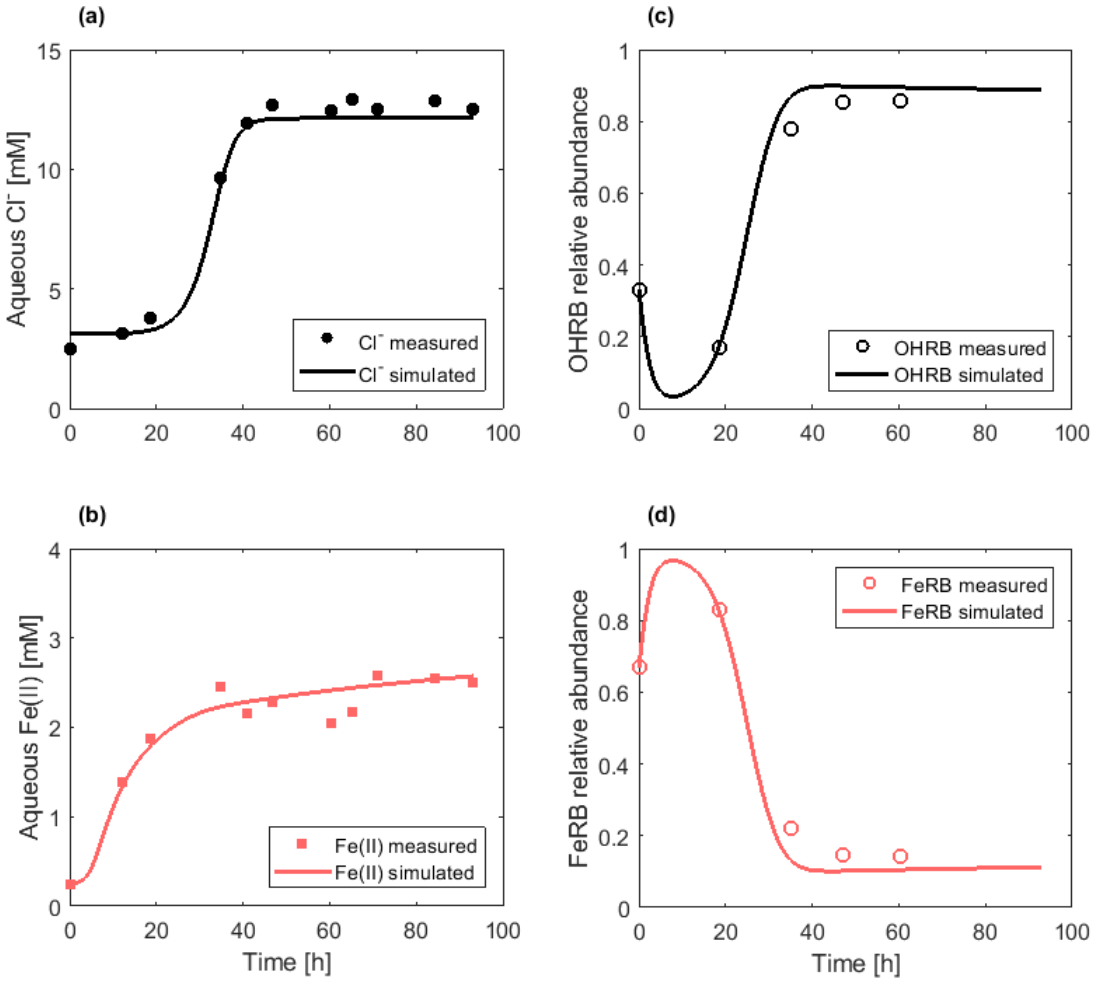

395

396 *Figure 4. OHRB and FeRB (Batch 2) experimental and simulated chloride and Fe(II) aqueous*
397 *concentrations (a and b) and OHRB and FeRB relative abundance (c and d). Data and simulation*
398 *results for the biological duplicate are included in the Supplementary Information (Figure S2).*

399 The Fe(II) concentration increases rapidly within the first 24 h of the experiment, and then increases
400 slowly throughout the rest of the experimental duration (Figure 4b). The concentration of Fe(II)
401 obtained at approximately 48 h, when PCE reduction was complete, is less than the Fe(III)
402 concentration added as Fe(III)-citrate because of Fe(III) speciation in the medium. Fe(II) reduction
403 is still ongoing at this time, since after the initial equilibration of the solution, less than 4% of the
404 Fe(III) was in a form that could be used by the bacteria. This phenomena has previously been
405 observed in experiments using a related bacterial strain (*Shewanella putrefaciens* strain CN32), in

406 which a half-velocity constant, $K_{S,FeRB,Fe3}$, was determined to be 2.9×10^{-3} M, based on the total
407 Fe(III) concentration and with lactate as the electron donor and carbon source (Liu et al., 2001). The
408 $K_{S,FeRB,Fe3}$ fit to our experiment were found to be 7.93×10^{-5} and 7.26×10^{-5} M in Batch 2 and its
409 biological duplicate. These values are two orders of magnitude lower, which is consistent with the
410 difference in magnitude between the bioavailable (this study) and total (Liu et al., 2001)
411 concentrations of the electron acceptor.

412 Because this batch includes multiple community members, the T-RFLP data shows the change in
413 the community over the duration of the experiment. Figure 4c and Figure 4d show that the FeRB
414 dominate the community for the first 24 h of the experiment, and the OHRB dominate throughout
415 the rest of the experimental duration. This correlates well with the rapid FeRB growth in the first 24
416 h of the experiment and the rapid OHRB growth between 24 and 40 h of the experiment. The
417 model, including the dynamics of the OHRB and FeRB, could well capture the observed molecular
418 data and the shift in dominance between the two microbial guilds during the timeframe of the
419 experiment.

420 **3.3 Two-Part Community: Organohalide- and Sulfate-Respiring Bacteria**

421 Batch 3, the two-part community that contained OHRB and SRB (Table 3 Column 3), inherently
422 contained more processes than the previous batches; the selected SRB bacteria is metabolically
423 versatile and the products from sulfate reduction react with Fe(III) and Fe(II). The model was again
424 able to simulate the sigmoid chloride accumulation curve (Figure 5a), and in this batch, repeated
425 chloride concentration values were obtained after approximately 60 h. The sulfate concentration
426 (Figure 5b) decreases slowly for the first 60 h of the experiment before decreasing rapidly between
427 approximately 60 and 65 h. This sulfate consumption by the SRB is reproduced well using the
428 kinetic constants determined by previous experiments (Noguera et al., 1998) that used hydrogen as
429 an electron donor. The relative abundance data (Figure 5d and Figure 5e) show that OHRB steadily

become dominant throughout the duration of the experiment. The simulation of the relative abundance data captures the general trend, in particular the repeated data points at the end of the T-RFLP time series data, which indicates that the model is able to capture the relative growth of the two guilds based on their yields once their electron acceptors have been completely consumed.

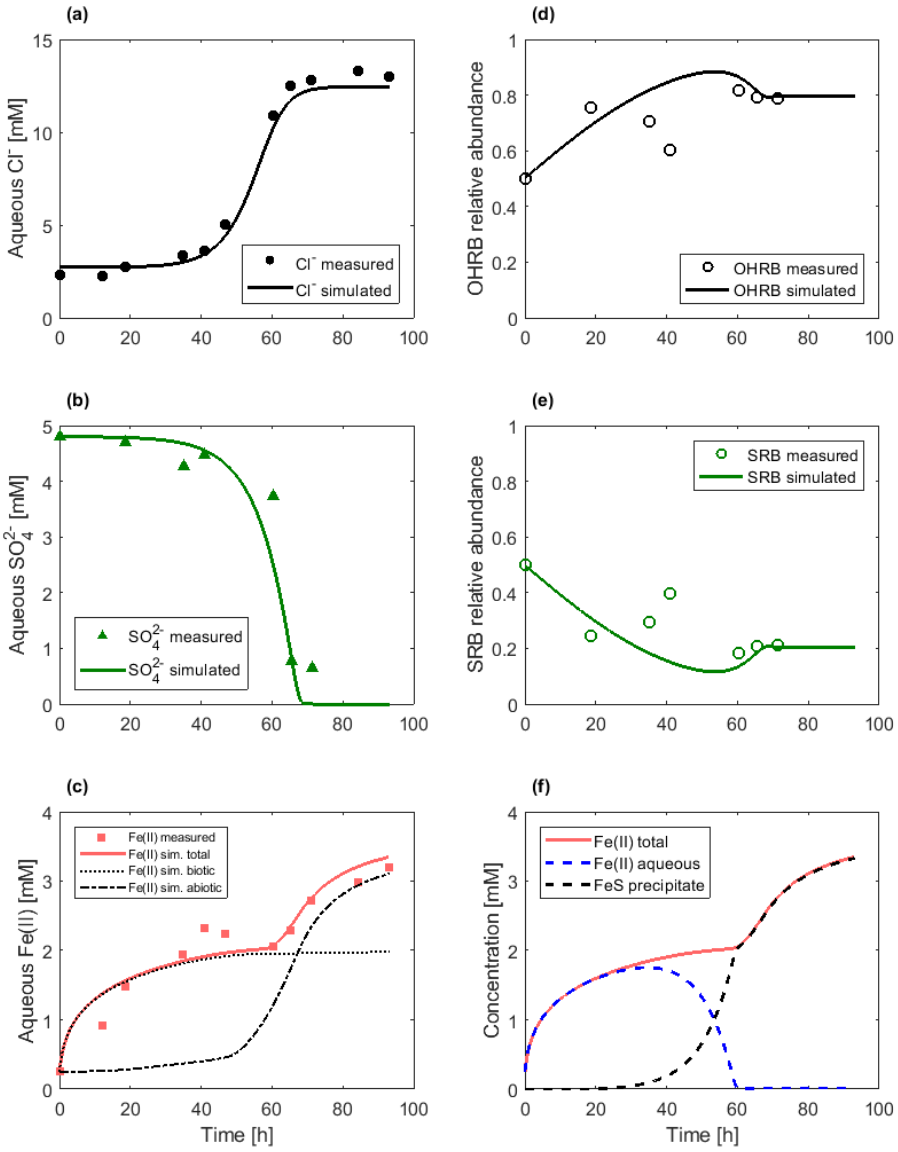

434

435 *Figure 5. OHRB and SRB (Batch 3) experimental and simulated chloride and sulfate aqueous*
436 *concentrations (a and b); experimental and simulated OHRB and SRB relative abundance (d and*
437 *e); experimental Fe(II) measurements and total simulated Fe(II)(red line), Fe(II) contributed by the*
438 *biotic reduction process by SRB (black dotted line), and the Fe(II) contributed by abiotic reduction*
439 *of Fe(III) by sulfide (black dashed line)(c); and simulated aqueous Fe(II) concentration (blue line)*
440 *and amorphous $FeS_{(s)}$ concentration (dashed black line)(f). Data and simulation results for the*
441 *biological duplicate are included in the Supplementary Information (Figure S3).*

442 The Fe(II) concentration measurements in Batch 3 (Figure 5c) appears to show two periods of fast
443 accumulation, the first within 0-20 h and the second within 60-70 h. This is in contrast to the Fe(II)
444 accumulation curve that results from Fe(III) respiration from FeRB in Batch 2 (Figure 4b), which
445 only showed an initial concentration increase in the first 24 h. In Batch 3, both biotic and abiotic
446 Fe(III) reduction to Fe(II) take place, and each process accounts for one of these observed increases.
447 Figure 5c demonstrates how neither abiotic nor biotic Fe(III) reduction alone is able to account for
448 the measured Fe(II) concentration, and that the Fe(II) accumulation curve is a composite of two
449 Fe(III) reduction processes. During the first 18 h of the experiment, the Fe(II) concentration has
450 risen by 1.2 mM and the sulfate concentration has decreased by 0.1 mM. Since 2 moles of Fe(II) are
451 produced per mole of sulfide consumed during abiotic Fe(III) reduction (Equation 11), another
452 process must be responsible for the observed increase in Fe(II). Likewise, if only first-order biotic
453 Fe(III) reduction by SRB is included in the model, then the elevated Fe(II) measurements at the end
454 of the time series are unable to be captured.

455 The SRB used in this experiment is capable of both Fe(III) and sulfate reduction. Biotic degradation
456 of Fe(III) by *Desulfovibrio* sp. has been documented to not result in cell synthesis and can be
457 modeled as a first-order process dependent on the concentration of bioavailable Fe(III) (Elias et al.,
458 2004). It has been posited that *Desulfovibrio* sp. reduce Fe(III) because it is a more favorable
459 electron acceptor (Zhou et al., 2017) or as protection against cell oxidation by compounds with a
460 higher redox potential than that of sulfate (Cypionka, 2000; Elias et al., 2004). Regardless of the
461 objective, it is evident that Fe(III) reduction proceeds first, followed by an apparent acceleration of
462 sulfate reduction after approximately 60 h.

463 The model also allows the simulation of the chemical reactions that occur as a result of sulfide
464 production via SRB respiration (Figure 5f). Though only the total Fe(II) concentration was
465 quantified, the formation of black precipitate in those batches that contained SRB was observed

after 24 h. The formation of precipitate was simulated using the standard thermodynamic PHREEQC database; the model corroborates what is visually observed and also shows that amorphous mackinawite, or $FeS_{(s)}$, begins to form after approximately 20 h. The simulation of Batch 3 shows that although sulfate reduction does occur relatively slowly throughout the first 40 h of the experiment (Figure 5b), $FeS_{(s)}$ is not the primary form of Fe(II) until after approximately 60 h of SRB growth. When sulfate is nearly depleted, all measured Fe(II) is bound as $FeS_{(s)}$.

3.4 Three-Part Community: Organohalide-, Fe(III)-, and Sulfate-Respiring Bacteria

In Batch 4, all three guilds were cultivated together (Table 3 Column 4), and all processes that were observed in each previous batch occurred together. The inoculum for this batch was comprised of the three guilds such that the initial cell count of each guild was the same as in the other three batches. Even when all three guilds are present, electron donor is still supplied in excess, and the lowest aqueous hydrogen concentration was 2.31×10^{-4} M.

The sigmoid chloride accumulation curve in Batch 4 (Figure 6a) is similar to those in Batches 1 (Figure 3a) and 2 (Figure 4a), as repeated concentration values were observed after approximately 48 hours. The Fe(II) measurements (Figure 6c) are similar to those found in Batch 3 (Figure 5c), in that there is a relatively fast increase to a concentration of about 2 mM within the first 20 h, and a second relatively fast increase in concentration at about 60 h. The sulfate curve, however, is slightly different in Batch 4 (Figure 6b) than in Batch 3 (Figure 5b). Although the sulfate disappears from the experiment at approximately 70 h in both batches, the decrease in measured sulfate appears to begin earlier and is more gradual in Batch 4 than in Batch 3. The model is able to accurately simulate both the chloride and sulfate curves as well as the Fe(II) composite curve.

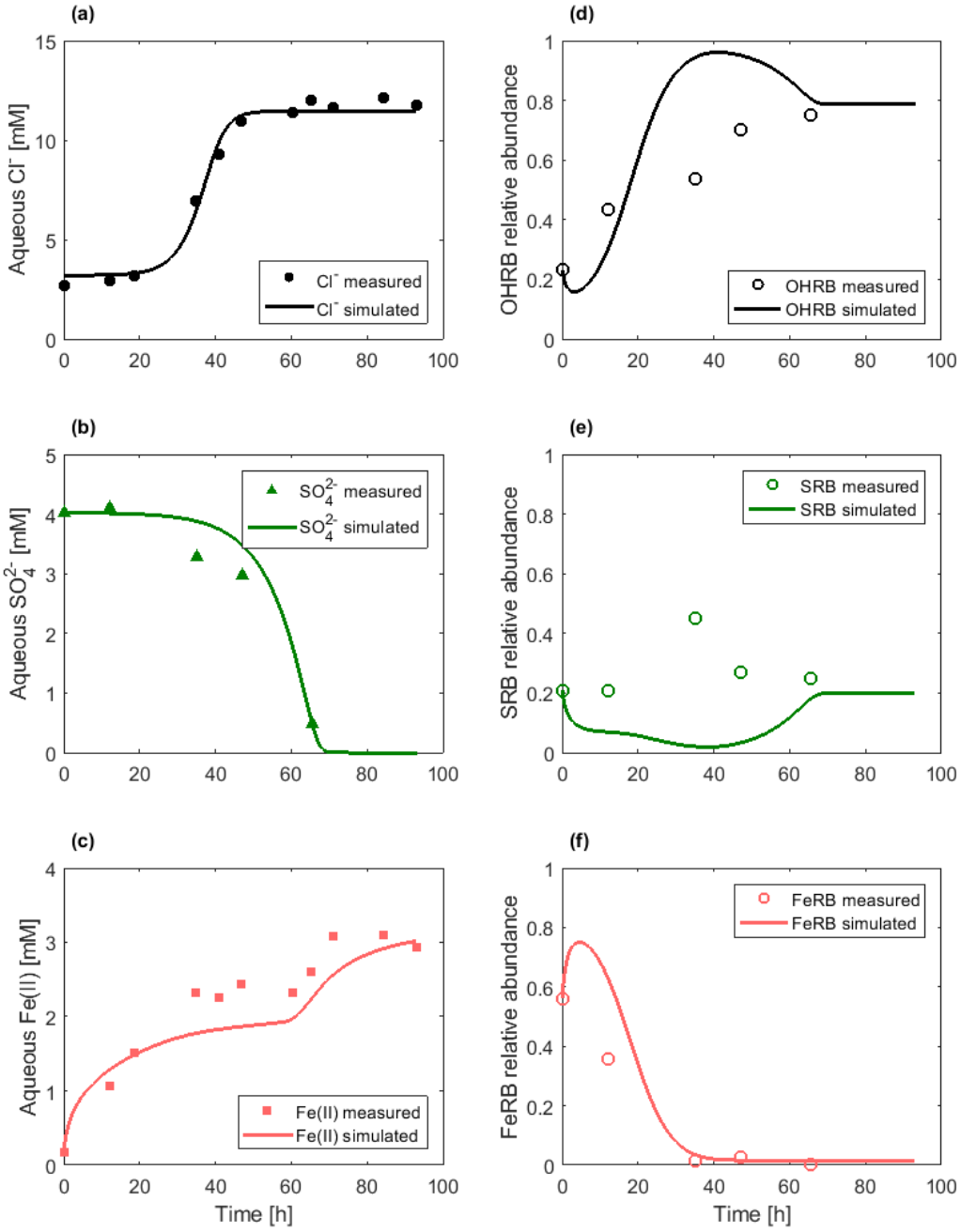

487

488 *Figure 6. OHRB, SRB, and FeRB (Batch 4) experimental and simulated chloride, sulfate, and total*
489 *Fe(II) aqueous concentrations (a, b, and c) and OHRB, SRB, and FeRB relative abundance (d, e,*
490 *and f). Data and simulation results for the biological duplicate are included in the Supplementary*
491 *Information (Figure S4).*

492 The T-RFLP relative abundance data show that the OHRB gradually grow to dominate the
493 microbial community throughout the time series while the SRB maintain a more or less steady
494 proportion and the FeRB rapidly decline to become a small proportion of the community. Just as in
495 Batches 2 and 3, the proportional community measurements (Figure 6d, e, and f) at the end of the
496 time series, after approximately 65 h, are captured for all three guilds, which is consistent with the
497 yield factors of the different guilds. More difficulties were encountered in the simulation of the
498 transient measurements of the community development. The model allows capturing the decrease of
499 FeRB, but overestimates the transient relative abundance for OHRB and underestimates for SRB.
500 This discrepancy may be because of the relative nature of the measurements that entails higher
501 uncertainties in this complex setup where all three guilds are simultaneously present (i.e., if one
502 measurement is inaccurate the others are affected), or it may indicate a process or metabolic
503 complementarity that is not represented in the current model formulation. It is evident from the
504 relative abundance data in Figure 6f that the FeRB do not thrive in relation to the other guilds in this
505 three guild scenario. It is possible that, in contrast to Batch 2, the consumption of the bioavailable
506 Fe(III) by the SRB and abiotic reduction is too great to allow the FeRB to access their electron
507 acceptor. However a change in the sulfate curve (Figure 6b) from Batch 3 (Figure 5b) is apparent,
508 in that the concentration decreases earlier in the experiment and more gradually. The Fe(III)
509 consumption by the FeRB, although not sufficient to allow FeRB to compete with the other guilds,
510 was enough to allow sulfate reduction by SRB to occur earlier, as evidenced by the observed and
511 simulated decrease of sulfate.

512 **3.5 Respiration Rates**

513 Investigating the batches comprehensively can yield knowledge about the way that Fe(III) and
514 sulfate reduction impact PCE degradation. Table 4 details the inverse fitting results for each batch
515 and its duplicate. All of the fitted k_{max} parameters for each guild and electron acceptor are within the

same order of magnitude, and it may appear that the bacteria behave similarly regardless of the community configuration. However, a visual comparison of the electron acceptor consumption rate can further illuminate how the community configuration impacts PCE degradation. In Figure 7, the rate of consumption of each electron acceptor in each batch configuration is displayed graphically. The highest point of each peak is the location of the maximum rate of consumption, and a narrow peak indicates a smaller time frame of respiration whereas a broader peak indicates respiration of the electron acceptor was sustained over a longer time.

Table 4. Fitted parameter model results. Estimated parameters for each batch duplicates are given in the second row for each batch; data and simulations for duplicates are included in the SI.

Parameter		$k_{max,OHRB}$ $mol_{PCE}\ cell^{-1}\ s^{-1}$	$k_{max,FeRB}$ $mol_{Fe3}\ cell^{-1}\ s^{-1}$	$k_{max,SRB}$ $mol_{SO4}\ cell^{-1}\ s^{-1}$	$K_{S,FeRB,Fe}$ $mol_{Fe3}\ L^{-1}$	$K_{S,SRB,SO4}$ $mol_{SO4}\ L^{-1}$	k_{FeAbio} $L^{0.5}\ mol^{-0.5} s^{-1}$
Batch	**1**	4.50×10^{-18}	--	--	--	--	--
		4.01×10^{-18}	--	--	--	--	--
	2	4.82×10^{-18}	1.82×10^{-17}	--	7.93×10^{-5}	--	--
		4.80×10^{-18}	1.97×10^{-17}	--	7.26×10^{-5}	--	--
	3	2.93×10^{-18}	--	8.40×10^{-18}	--	--	2.97×10^{-4}
		3.35×10^{-18}	--	8.11×10^{-18}	--	--	4.31×10^{-4}
	4	4.13×10^{-18}	2.18×10^{-17}	8.45×10^{-17}	--	3.51×10^{-4}	--
		3.98×10^{-18}	1.68×10^{-17}	1.60×10^{-17}	--	2.91×10^{-3}	--

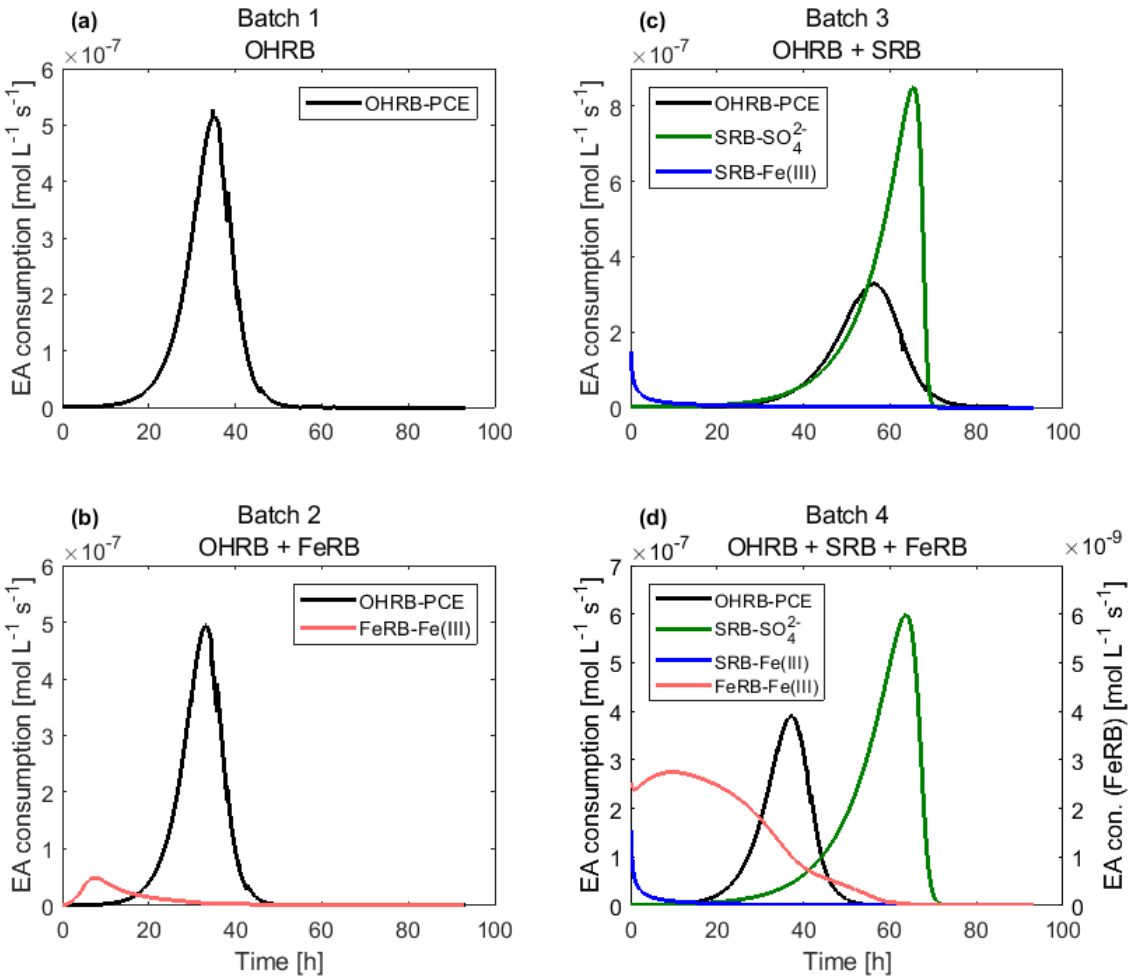

525

526 *Figure 7. Comsumption rates for electron acceptors in batches with Batch 1: OHRB (a), Batch 2:*

527 *OHRB + FeRB (b), Batch 3: OHRB + SRB (c), and Batch 4: OHRB + FeRB + SRB (d).*

528 When comparing Batches 1 and 2, in which the OHRB consortium was present alone and in

529 combination with FeRB (Figure 7a and b), it is evident that there is no appreciable difference

530 between the degradation of PCE when the FeRB are and are not present, as the shape of the PCE

531 consumption peak is similar in both shape and height in both batches. The OHRB appear to behave

532 no differently whether reduction by FeRB occurs or not. This may be due to the Fe(III) speciation

533 and subsequent electron acceptor bioavailability limitation on FeRB respiration.

534 The OHRB behavior in Batch 3 is noticeably different from that of Batches 1 and 2 (Figure 7c). It is

535 evident that PCE degradation proceeds much less rapidly, as the maximum specific rate of PCE

consumption is 65% of that observed in Batch 1 and 61% of that observed in Batch 2 (Figure 7a and b). The OHRB only begin to consume PCE concurrently with sulfate consumption as shown by the simulated rate curves of the 2 bacterial guilds. Such a correlation between PCE degradation and sulfate reduction has also been found in other studies (Aulenta et al., 2008; Berggren et al., 2013; Mao et al., 2015). Furthermore, in Batch 4 (Figure 7d) it appears that Fe(III) reduction by FeRB can enhance PCE reduction by OHRB, although the maximum specific degradation rate is still subdued compared to that of Batches 1 and 2. This may highlight the necessity to consider the biodiversity of the entire microbial community during bioremediation application (Aulenta et al., 2007), rather than focus on organohalide-respiring bacteria.

4. Conclusion

In this study we have proposed a modeling approach, based on MATLAB®-PHREEQC coupling, to interpret biological assays in which microbial dynamics, mass transfer processes, and geochemical reactions can affect the degradation of organic contaminants. We performed batch experiments of increasing ecological complexity on the impact of iron and sulfate reduction on PCE reductive dehalogenation, and we used the proposed model to interpret the experimental observations. The model allowed us to quantify the kinetics of the different bacterial guilds and to quantitatively evaluate the effects of the physical, chemical and biological processes that occurred in the multi-phase batch setups. Furthermore, the model could calculate the respiration rate throughout the experimental duration, and thus the change in rate could be depicted and compared across different community compositions. The rate of PCE degradation appeared unaffected by Fe(III) respiration by FeRB, which may be due to Fe(III) bioavailability and the low Fe(III) respiration rate. Sulfate respiration by SRB did delay and decrease the PCE degradation rate; however, as was seen in the 3-part community simulation, this effect was moderated by the presence of FeRB.

559 The focus of the study was one-step dehalorespiration of PCE, however the experimental design
560 and modeling tool could be extended to more complex systems, such as multi-step degradation of
561 chlorinated ethenes and investigation of microbial competition during the transformation of further
562 PCE daughter products *cis*-dichloroethene and vinyl chloride. The number of guilds considered
563 could be expanded to include, for instance, fermenting organisms. Both the experimental and
564 modeling approach can be adapted to investigate degradation of different organic contaminants and
565 microbial community interactions in two-, three-, and four-phase systems and with sample removal
566 not limited to the aqueous phase. For instance, volatile compounds may be sampled and measured
567 directly from the gaseous phase.

568 The modeling tool developed in this study has a flexible structure that can be easily transferable to
569 other domains with different properties and dimensionality. For instance the reaction modules
570 developed in this work could be adapted to investigate community interactions between the same
571 microbial guilds and the feedback effects of aquatic chemistry in flow-through microcosms (Bauer
572 et al., 2009b). This will allow exploring the combined effects of solute transport processes,
573 geochemical reactions, contaminant degradation and ecological interactions in multidimensional
574 systems in which the physical and chemical heterogeneity will impact the biogeochemical processes
575 and the spatial distribution of different bacterial guilds in flow-through porous media. Similarly, the
576 reaction modules that describe microbial community and biogeochemical interactions could be
577 applied in reactive transport simulators at the field scale to help interpret the behavior of
578 groundwater contaminant plumes (e.g., Parker et al., 2008; Shani et al., 2013; Van Breukelen and
579 Rolle, 2012).

580

Acknowledgements

This study was funded by a DTU alliance PhD scholarship granted to Alexandra Murray. Massimo Rolle acknowledges the support of the Independent Research Fund Denmark (grant DFF-7017-00130). Constructive comments from two anonymous reviewers helped to improve the quality of the manuscript.

586 **References**

587 Abe, Y., Aravena, R., Zopfi, J., Parker, B., Hunkeler, D., 2009. Evaluating the fate of chlorinated
588 ethenes in streambed sediments by combining stable isotope, geochemical and microbial
589 methods. J. Contam. Hydrol. 107, 10–21. https://doi.org/10.1016/j.jconhyd.2009.03.002

590 Aeppli, C., Berg, M., Cirpka, O.A., Holliger, C., Schwarzenbach, R.P., Hofstetter, T.B., 2009.
591 Influence of mass-transfer limitations on carbon isotope fractionation during microbial
592 dechlorination of trichloroethene. Environ. Sci. Technol. 43, 8813–8820.
593 https://doi.org/10.1021/es901481b

594 Amos, B.K., Christ, J.A., Abriola, L.M., Pennell, K.D., Löffler, F.E., 2007. Experimental evaluation
595 and mathematical modeling of microbially enhanced tetrachloroethene (PCE) dissolution.
596 Environ. Sci. Technol. 41, 963–970. https://doi.org/10.1021/es061438n

597 Appelo, C.A.J., Postma, D., 2005. Geochemistry, groundwater and pollution, Second. ed. A.A.
598 Balkema Publishers, Leiden.

599 Aulenta, F., Beccari, M., Majone, M., Papini, M.P., Tandoi, V., 2008. Competition for H2 between
600 sulfate reduction and dechlorination in butyrate-fed anaerobic cultures. Process Biochem. 43,
601 161–168. https://doi.org/10.1016/j.procbio.2007.11.006

602 Aulenta, F., Pera, A., Rossetti, S., Petrangeli Papini, M., Majone, M., 2007. Relevance of side
603 reactions in anaerobic reductive dechlorination microcosms amended with different electron
604 donors. Water Res 41, 27–38. https://doi.org/10.1016/j.watres.2006.09.019

605 Badziong, W., Thauer, R.K., 1978. Growth yields and growth rates of Desulfovibrio vulgaris
606 (Marburg) growing on hydrogen plus sulfate and hydrogen plus thiosulfate as the sole energy
607 sources. Arch. Microbiol. 117, 209–214. https://doi.org/10.1007/bf00402310

608 Balkwill, D.L., Leach, F.R., Wilson, J.T., Mcnabb, J.F., White, D.C., 1988. Equivalence of
609 Microbial Biomass Measures Based on Membrane Lipid and Cell Wall Components ,
610 Adenosine Triphosphate , and Direct Counts in Subsurface Aquifer Sediments Abstract . 73–
611 84.

612 Bauer, R.D., Rolle, M., Bauer, S., Eberhardt, C., Grathwohl, P., Kolditz, O., Meckenstock, R.U.,
613 Griebler, C., 2009. Enhanced biodegradation by hydraulic heterogeneities in petroleum
614 hydrocarbon plumes. J. Contam. Hydrol. 105, 56–68.
615 https://doi.org/10.1016/j.jconhyd.2008.11.004

616 Bauer, R.D., Rolle, M., Kürzinger, P., Grathwohl, P., Meckenstock, R.U., Griebler, C., 2009. Two-
617 dimensional flow-through microcosms – Versatile test systems to study biodegradation
618 processes in porous aquifers. J. Hydrol. 369, 284–295.
619 https://doi.org/10.1016/j.jhydrol.2009.02.037

620 Berggren, D.R. V, Marshall, I.P.G., Azizian, M.F., Spormann, A.M., Semprini, L., 2013. Effects of
621 sulfate reduction on the bacterial community and kinetic parameters of a dechlorinating culture
622 under chemostat growth conditions. Environ. Sci. Technol. 47, 1879–1886.
623 https://doi.org/10.1021/es304244z

624 Buchner, D., Jin, B., Ebert, K., Rolle, M., Elsner, M., Haderlein, S.B., 2016. Experimental
625 Determination of Isotope Enrichment Factors – Bias from Mass Removal by Repetitive
626 Sampling. Environ. Sci. Technol. acs.est.6b03689. https://doi.org/10.1021/acs.est.6b03689

627 Buttet, G.F., Holliger, C., Maillard, J., 2013. Functional genotyping of Sulfurospirillum spp. in
628 mixed cultures allowed the identification of a new tetrachloroethene reductive dehalogenase.
629 Appl. Environ. Microbiol. 79. https://doi.org/10.1128/AEM.02312-13

630 Buttet, G.F., Murray, A.M., Goris, T., Burion, M., Jin, B., Rolle, M., Holliger, C., Maillard, J.,
631 2018. Coexistence of two distinct Sulfurospirillum populations respiring tetrachloroethene-
632 genomic and kinetic considerations. FEMS Microbiol. Ecol. 94, 1–11.
633 https://doi.org/10.1093/femsec/fiy018

634 Chambon, J.C., Bjerg, P.L., Scheutz, C., Bælum, J., Jakobsen, R., Binning, P.J., 2013. Review of
635 reactive kinetic models describing reductive dechlorination of chlorinated ethenes in soil and
636 groundwater. Biotechnol. Bioeng. 110, 1–23. https://doi.org/10.1002/bit.24714

637 Charlton, S.R., Parkhurst, D.L., 2011. Modules based on the geochemical model PHREEQC for use
638 in scripting and programming languages. Comput. Geosci. 37, 1653–1663.
639 https://doi.org/10.1016/j.cageo.2011.02.005

640 Cypionka, H., 2000. Oxygen respiration by Desulfovibrio species. Annu. Rev. Microbiol. 54, 827–
641 48.

642 Daugulis, A.J., 2001. Two-phase partitioning bioreactors: A new technology platform for
643 destroying xenobiotics. Trends Biotechnol. 19, 457–462. https://doi.org/10.1016/S0167-
644 7799(01)01789-9

645 Déziel, E., Comeau, Y., Villemur, R., 1999. Two-liquid-phase bioreactors for enhanced degradation
646 of hydrophobic/toxic compounds. Biodegradation 10, 219–233.
647 https://doi.org/10.1023/A:1008311430525

648 Elias, D.A., Suflita, J.M., McInerney, M.J., Krumholz, L.R., 2004. Periplasmic Cytochrome c3 of
649 *Desulfovibrio vulgaris* is directly involved in H2-mediated metal but not sulfate reduction.
650 Appl. Environ. Microbiol. 70, 413–420. https://doi.org/10.1128/AEM.70.1.413

651 Fredrickson, J.K., Romine, M.F., Beliaev, A.S., Auchtung, J.M., Driscoll, M.E., Gardner, T.S.,

652 Nealson, K.H., Osterman, A.L., Pinchuk, G., Reed, J.L., Rodionov, D. a, Rodrigues, J.L.M.,
653 Saffarini, D. a, Serres, M.H., Spormann, A.M., Zhulin, I.B., Tiedje, J.M., 2008. Towards
654 environmental systems biology of *Shewanella*. Nat. Rev. Microbiol. 6, 592–603.
655 https://doi.org/10.1038/nrmicro1947

656 Gadd, G.M., 2010. Metals, minerals and microbes: Geomicrobiology and bioremediation.
657 Microbiology 156, 609–643. https://doi.org/10.1099/mic.0.037143-0

658 Haas, J.R., Dichristina, T.J., 2002. Effects of FE(III) chemical speciation on dissimilatory FE(III)
659 reduction by shewanella putrefaciens. Environ. Sci. Technol. 36, 373–380.
660 https://doi.org/10.1021/es0109287

661 Haberer, C.M., Muniruzzaman, M., Grathwohl, P., Rolle, M., 2015. Diffusive–Dispersive and
662 Reactive Fronts in Porous Media: Iron(II) Oxidation at the Unsaturated–Saturated Interface.
663 Vadose Zo. J. 14, 1–14. https://doi.org/10.2136/vzj2014.07.0091

664 Hamonts, K., Kuhn, T., Vos, J., Maesen, M., Kalka, H., Smidt, H., Springael, D., Meckenstock,
665 R.U., Dejonghe, W., 2012. Temporal variations in natural attenuation of chlorinated aliphatic
666 hydrocarbons in eutrophic river sediments impacted by a contaminated groundwater plume.
667 Water Res. 46, 1873–1888. https://doi.org/10.1016/j.watres.2012.01.001

668 Heidelberg, J.F., Paulsen, I.T., Nelson, K.E., Gaidos, E.J., Nelson, W.C., Read, T.D., Eisen, J. a,
669 Seshadri, R., Ward, N., Methe, B., Clayton, R. a, Meyer, T., Tsapin, A., Scott, J., Beanan, M.,
670 Brinkac, L., Daugherty, S., DeBoy, R.T., Dodson, R.J., Durkin, a S., Haft, D.H., Kolonay,
671 J.F., Madupu, R., Peterson, J.D., Umayam, L. a, White, O., Wolf, A.M., Vamathevan, J.,
672 Weidman, J., Impraim, M., Lee, K., Berry, K., Lee, C., Mueller, J., Khouri, H., Gill, J.,
673 Utterback, T.R., McDonald, L. a, Feldblyum, T. V, Smith, H.O., Venter, J.C., Nealson, K.H.,
674 Fraser, C.M., 2002. Genome sequence of the dissimilatory metal ion-reducing bacterium

675 *Shewanella oneidensis*. Nat. Biotechnol. 20, 1118–1123. https://doi.org/10.1038/nbt749

676 Heidelberg, J.F., Seshadri, R., Haveman, S.A., Hemme, C.L., Paulsen, I.T., Kolonay, J.F., Eisen,
677 J.A., Ward, N., Methe, B., Brinkac, L.M., Daugherty, S.C., Deboy, R.T., Dodson, R.J., Durkin,
678 A.S., Madupu, R., Nelson, W.C., Sullivan, S.A., Fouts, D., Haft, D.H., Selengut, J., Peterson,
679 J.D., Davidsen, T.M., Zafar, N., Zhou, L., Radune, D., Dimitrov, G., Hance, M., Tran, K.,
680 Khouri, H., Gill, J., Utterback, T.R., Feldblyum, T. V, Wall, J.D., Voordouw, G., Fraser, C.M.,
681 2004. The genome sequence of the anaerobic, sulfate-reducing bacterium *Desulfovibrio*
682 *vulgaris* Hildenborough. Nat. Biotechnol. 22, 554–559. https://doi.org/10.1038/nbt959

683 Holliger, C., Schraa, G., Stams, A.J.M., Zehnder, A.J.B., 1993. A highly purified enrichment
684 culture couples the reductive dechlorination of tetrachloroethene to growth. Appl. Environ.
685 Microbiol. 59, 2991–2997.

686 Imfeld, G., Nijenhuis, I., Nikolausz, M., Zeiger, S., Paschke, H., Drangmeister, J., Grossmann, J.,
687 Richnow, H.H., Weber, S., 2008. Assessment of in situ degradation of chlorinated ethenes and
688 bacterial community structure in a complex contaminated groundwater system. Water Res. 42,
689 871–882. https://doi.org/10.1016/j.watres.2007.08.035

690 Jakobsen, R., 2007. Redox microniches in groundwater: A model study on the geometric and
691 kinetic conditions required for concomitant Fe oxide reduction, sulfate reduction, and
692 methanogenesis. Water Resour. Res. 43. https://doi.org/10.1029/2006WR005663

693 Jin, B., Haderlein, S.B., Rolle, M., 2013. Integrated carbon and chlorine isotope modeling:
694 Applications to chlorinated aliphatic hydrocarbons dechlorination. Environ. Sci. Technol. 47,
695 1443–1451. https://doi.org/10.1021/es304053h

696 Jin, B., Rolle, M., 2016. Joint interpretation of enantiomer and stable isotope fractionation for chiral

pesticides degradation. Water Res. 105, 178–186. https://doi.org/10.1016/j.watres.2016.08.057

Kampara, M., Thullner, M., Richnow, H.H., Harms, H., Wick, L.Y., 2008. Impact of Bioavailability Restrictions on Microbially Induced Stable Isotope Fractionation. 2. Experimental Evidence. Environ. Sci. Technol. 42, 6544–6551. https://doi.org/Doi 10.1021/Es702781x

Kotik, M., Davidová, A., Voříšková, J., Baldrian, P., 2013. Bacterial communities in tetrachloroethene-polluted groundwaters: a case study. Sci. Total Environ. 454–455, 517–27. https://doi.org/10.1016/j.scitotenv.2013.02.082

Kouznetsova, I., Mao, X., Robinson, C., Barry, D. a., Gerhard, J.I., McCarty, P.L., 2010. Biological reduction of chlorinated solvents: Batch-scale geochemical modeling. Adv. Water Resour. 33, 969–986. https://doi.org/10.1016/j.advwatres.2010.04.017

Liu, C., Zachara, J.M., Gorby, Y.A., Szecsody, J.E., Brown, C.F., 2001. Microbial reduction of Fe(III) and sorption/precipitation of Fe(II) on *Shewanella putrefaciens* strain CN32. Environ. Sci. Technol. 35, 1385–1393. https://doi.org/10.1021/es0015139

Malaguerra, F., Chambon, J.C., Bjerg, P.L., Scheutz, C., Binning, P.J., 2011. Development and sensitivity analysis of a fully kinetic model of sequential reductive dechlorination in groundwater. Environ. Sci. Technol. 45, 8395–8402. https://doi.org/10.1021/es201270z

Mao, X., Stenuit, B., Polasko, A., Alvarez-Cohen, L., 2015. Efficient metabolic exchange and electron transfer within a syntrophic trichloroethene-degrading coculture of Dehalococcoides mccartyi 195 and Syntrophomonas wolfei. Appl. Environ. Microbiol. 81, 2015–2024. https://doi.org/10.1128/AEM.03464-14

Marcus, I.M., Wilder, H.A., Quazi, S.J., Walker, S.L., 2013. Linking microbial community structure to function in representative simulated systems. Appl. Environ. Microbiol. 79, 2552–

719 2559. https://doi.org/10.1128/AEM.03461-12

720 Meckenstock, R.U., Elsner, M., Griebler, C., Lueders, T., Stumpp, C., Dejonghe, W., Bastiaens,
721 L.L., Springael, D., Smolders, E., Boon, N., Agathos, S.N., Sorensen, S.R., Aamand, J.,
722 Albrechtsen, H.J., Bjerg, P.L., Schmidt, S., Huang, W.E., Van Breukelen, B.M., 2015.
723 Biodegradation: Updating the concepts of control for microbial clean-up in contaminated
724 aquifers. Environ. Sci. Technol. 49, 7073–7081. https://doi.org/10.1021/acs.est.5b00715

725 Muniruzzaman, M., Rolle, M., 2016. Modeling multicomponent ionic transport in groundwater with
726 IPhreeqc coupling: Electrostatic interactions and geochemical reactions in homogeneous and
727 heterogeneous domains. Adv. Water Resour. 98, 1–15.
728 https://doi.org/10.1016/j.advwatres.2016.10.013

729 Murray, A., Ottosen, C.B., Maillard, J., Holliger, C., Johansen, A., Brabæk, L., Kristensen, I.L.,
730 Zimmermann, J., Hunkeler, D., Broholm, M.M., n.d. Chlorinated ethene plume evolution after
731 source thermal remediation: determination of degradation rates and mechanisms. J. Contam.
732 Hydrol.

733 Noguera, D., Brusseau, G., Rittmann, B., Stahl, D., 1998. A unified model describing the role of
734 hydrogen in the growth of desulfovibrio vulgaris under different environmental conditions.
735 Biotechnol. Bioeng. 59, 732–46. https://doi.org/10.1002/(sici)1097-
736 0290(19980920)59:6<732::aid-bit10>3.3.co;2-2

737 Park, H.S., Lin, S., Voordouw, G., 2008. Ferric iron reduction by *Desulfovibrio vulgaris*
738 Hildenborough wild type and energy metabolism mutants. Antonie van Leeuwenhoek, Int. J.
739 Gen. Mol. Microbiol. 93, 79–85. https://doi.org/10.1007/s10482-007-9181-3

740 Parker, B.L., Chapman, S.W., Guilbeault, M.A., 2008. Plume persistence caused by back diffusion

741 from thin clay layers in a sand aquifer following TCE source-zone hydraulic isolation. J.
742 Contam. Hydrol. 102, 86–104. https://doi.org/10.1016/j.jconhyd.2008.07.003

743 Parkhurst, D.L., Appelo, C.A.J., 2013. Description of input and examples for PHREEQC Version 3
744 — A computer program for speciation, batch-reaction, one-dimensional transport, and inverse
745 geochemical calculations. U.S. Geol. Surv. Tech. Methods, B. 6, chapter A43 6–43A.
746 https://doi.org/10.1016/0029-6554(94)90020-5

747 Postma, D., Jakobsen, R., 1996. Redox zonation: Equilibrium constraints on the Fe(III)/SO4-
748 reduction interface. Geochim. Cosmochim. Acta 60, 3169–3175.

749 Poulton, S.W., Krom, M.D., Raiswell, R., 2004. A revised scheme for the reactivity of iron
750 (oxyhydr) oxide minerals towards dissolved sulfide. Geochim. Cosmochim. Acta 68, 3703–
751 3715. https://doi.org/10.1016/j.gca.2004.03.012

752 Prommer, H., Anneser, B., Rolle, M., Einsiedl, F., Griebler, C., 2009. Biogeochemical and isotopic
753 gradients in a BTEX/PAH contaminant plume: Model-based interpretation of a high-resolution
754 field data set. Environ. Sci. Technol. 43, 8206–8212. https://doi.org/10.1021/es901142a

755 Remoundaki, E., Kousi, P., Joulian, C., Battaglia-Brunet, F., Hatzikioseyian, A., Tsezos, M., 2008.
756 Characterization, morphology and composition of biofilm and precipitates from a sulphate-
757 reducing fixed-bed reactor. J. Hazard. Mater. 153, 514–524.
758 https://doi.org/10.1016/j.jhazmat.2007.08.094

759 Rickard, D., 1995. Kinetics of FeS precipitation: Part 1. Competing reaction mechanisms. Geochim.
760 Cosmochim. Acta 59, 4367–4379. https://doi.org/10.1016/0016-7037(95)00251-T

761 Rickard, D., Luther, G.W., 2007. Chemistry of iron sulfides, Chemical Reviews.
762 https://doi.org/10.1021/cr0503658

763 Rittmann, B.E., McCarty, P.L., 2001. Environmental Biotechnology: Principles and Applications,
764 First. ed. McGraw-Hill, New York.

765 Rolle, M., Chiogna, G., Bauer, R., Griebler, C., Grathwohl, P., 2010. Isotopic fractionation by
766 transverse dispersion: Flow-through microcosms and reactive transport modeling study.
767 Environ. Sci. Technol. 44, 6167–6173. https://doi.org/10.1021/es101179f

768 Rolle, M., Kitanidis, P.K., 2014. Effects of compound-specific dilution on transient transport and
769 solute breakthrough: A pore-scale analysis. Adv. Water Resour. 71, 186–199.
770 https://doi.org/10.1016/j.advwatres.2014.06.012

771 Rolle, M., Sprocati, R., Masi, M., Jin, B., Muniruzzaman, M., 2018. Nernst-Planck-based
772 Description of Transport, Coulombic Interactions, and Geochemical Reactions in Porous
773 Media: Modeling Approach and Benchmark Experiments. Water Resour. Res. 54, 3176–3195.
774 https://doi.org/10.1002/2017WR022344

775 Schneidewind, U., Haest, P.J., Atashgahi, S., Maphosa, F., Hamonts, K., Maesen, M., Calderer, M.,
776 Seuntjens, P., Smidt, H., Springael, D., Dejonghe, W., 2014. Kinetics of dechlorination by
777 Dehalococcoides mccartyi using different carbon sources. J. Contam. Hydrol. 157, 25–36.
778 https://doi.org/10.1016/j.jconhyd.2013.10.006

779 Scholz-Muramatsu, H., Neumann, A., Messmer, M., Moore, E., Diekert, G., 1995. Isolation and
780 characterization of Dehalospirillum multivorans gen . nov ., sp . nov ., a tetrachloroethene-
781 utilizing , strictly anaerobic bacterium. Arch. Microbiol. 163, 48–56.

782 Shani, N., Rossi, P., Holliger, C., 2013. Correlations between environmental variables and bacterial
783 community structures suggest Fe(III) and vinyl chloride reduction as antagonistic terminal
784 electron-accepting processes. Environ. Sci. Technol. 47, 6836–6845.

https://doi.org/10.1021/es304017s

Tang, Y.J., Meadows, A.L., Keasling, J.D., 2007. A kinetic model describing *Shewanella oneidensis* MR-1 growth, substrate consumption, and product secretion. Biotechnol. Bioeng. 96, 125–133. https://doi.org/10.1002/bit

Tao, X., Li, Y., Huang, H., Chen, Y., Liu, P., Li, X., 2014. *Desulfovibrio vulgaris* Hildenborough prefers lactate over hydrogen as electron donor. Ann. Microbiol. 64, 451–457. https://doi.org/10.1007/s13213-013-0675-0

Thullner, M., Fischer, A., Richnow, H.H., Wick, L.Y., 2012. Influence of mass transfer on stable isotope fractionation. Appl. Microbiol. Biotechnol. 97, 441–452. https://doi.org/10.1007/s00253-012-4537-7

Thullner, M., Kampara, M., Richnow, H.H., Harms, H., Wick, L.Y., 2008. Impact of Bioavailability Restrictions on Microbially Induced Stable Isotope Fractionation. 1. Theoretical Calculation. Environ. Sci. Technol. 42, 6544–6551. https://doi.org/Doi 10.1021/Es702781x

Van Breukelen, B.M., Rolle, M., 2012. Transverse hydrodynamic dispersion effects on isotope signals in groundwater chlorinated solvents plumes. Environ. Sci. Technol. 46, 7700–7708. https://doi.org/10.1021/es301058z

Van Breukelen, B.M., Thouement, H.A.A., Stack, P.E., Vanderford, M., Philp, P., Kuder, T., 2017. Modeling 3D-CSIA data: Carbon, chlorine, and hydrogen isotope fractionation during reductive dechlorination of TCE to ethene. J. Contam. Hydrol. 204, 79–89. https://doi.org/10.1016/j.jconhyd.2017.07.003

Viollier, E., Inglett, P.W., Hunter, K., Roychoudhury, A.N., Van Cappellen, P., 2000. The ferrozine method revisited: Fe(II)/Fe(III) determination in natural waters. Appl. Geochemistry 15, 785–

790. https://doi.org/10.1016/S0883-2927(99)00097-9

Wade, M.J., Harmand, J., Benyahia, B., Bouchez, T., Chaillou, S., Cloez, B., Godon, J.J., Moussa Boudjemaa, B., Rapaport, A., Sari, T., Arditi, R., Lobry, C., 2016. Perspectives in mathematical modelling for microbial ecology. Ecol. Modell. 321, 64–74. https://doi.org/10.1016/j.ecolmodel.2015.11.002

Weatherill, J.J., Atashgahi, S., Schneidewind, U., Krause, S., Ullah, S., Cassidy, N., Rivett, M.O., 2018. Natural attenuation of chlorinated ethenes in hyporheic zones: A review of key biogeochemical processes and in-situ transformation potential. Water Res. 128, 362–382. https://doi.org/10.1016/j.watres.2017.10.059

Wells, G.F., Park, H.D., Eggleston, B., Francis, C.A., Criddle, C.S., 2011. Fine-scale bacterial community dynamics and the taxa-time relationship within a full-scale activated sludge bioreactor. Water Res. 45, 5476–5488. https://doi.org/10.1016/j.watres.2011.08.006

Wissmeier, L., Barry, D.A., 2011. Simulation tool for variably saturated flow with comprehensive geochemical reactions in two- and three-dimensional domains. Environ. Model. Softw. 26, 210–218. https://doi.org/10.1016/j.envsoft.2010.07.005

Xu, G., Lu, Q., Yu, L., Wang, S., 2019. Tetrachloroethene Primes Reductive Dechlorination of Polychlorinated Biphenyls in a River Sediment Microcosm. Water Res. 152, 87–95. https://doi.org/10.1016/j.watres.2018.12.061

Yu, S., Semprini, L., 2004. Kinetics and modeling of reductive dechlorination at high PCE and TCE concentrations. Biotechnol. Bioeng. 88, 451–464. https://doi.org/10.1002/bit.20260

Yu, S., Semprini, L., 2002. Comparison of trichloroethylene reductive dehalogenation by microbial communities stimulated on silicon-based organic compounds as slow-release anaerobic

829 substrates. Water Res. 36, 4985–4996. https://doi.org/10.1016/S0043-1354(02)00222-1

830 Zhou, C., Vannela, R., Hayes, K.F., Rittmann, B.E., 2014. Effect of growth conditions on microbial
831 activity and iron-sulfide production by Desulfovibrio vulgaris. J. Hazard. Mater. 272, 28–35.
832 https://doi.org/10.1016/j.jhazmat.2014.02.046

833 Zhou, C., Zhou, Y., Rittmann, B.E., 2017. Reductive precipitation of sulfate and soluble Fe(III) by
834 *Desulfovibrio vulgaris*: Electron donor regulates intracellular electron flow and nano-FeS
835 crystallization. Water Res. 119, 91–101. https://doi.org/10.1016/j.watres.2017.04.044

836